
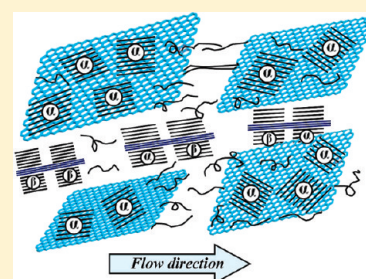


Graphene Nanosheets and Shear Flow Induced Crystallization in Isotactic Polypropylene Nanocomposites

Jia-Zhuang Xu,[†] Chen Chen,[‡] Yan Wang,[†] Hu Tang,[†] Zhong-Ming Li,^{*,†} and Benjamin S. Hsiao^{*,§}[†]College of Polymer Science and Engineering and State Key Laboratory of Polymer Materials Engineering, Sichuan University, Chengdu 610065, China[‡]Analytical and Testing Center, Sichuan University, Chengdu, 610065, China[§]Department of Chemistry, Stony Brook University, Stony Brook, New York 11794-3400, United States Supporting Information

ABSTRACT: Combined effects of graphene nanosheets (GNSs) and shear flow on the crystallization behavior of isotactic polypropylene (iPP) were investigated by in-situ synchrotron wide-angle X-ray diffraction (WAXD) and small-angle X-ray scattering (SAXS) techniques. For crystallization under quiescent condition (at 145 °C), the half-crystallization time ($t_{1/2}$) of nanocomposites containing 0.05 and 0.1 wt % GNSs was reduced to at least 50% compared to that of neat iPP, indicating the high nucleation ability of GNSs. The crystallization rate of iPP was directly proportional to the GNS content. Under a relatively weak shear flow (at a rate of 20 s⁻¹ for 5 s duration) and a low degree of supercooling, the neat iPP exhibited an isotropic structure due to the relaxation of row nuclei. However, visible anisotropic crystals appeared in sheared iPP/GNSs nanocomposites, indicating that GNSs induced a network structure hindering the mobility of iPP chains and allowing the survival of oriented row nuclei for a long period of time. The presence of GNSs clearly enhanced the effects of shear-induced nucleation as well as orientation of iPP crystals. Two kinds of nucleating origins coexisted in the sheared nanocomposite melt: heterogeneous nucleating sites initiated by GNSs and homogeneous nucleating sites (row nuclei) induced by shear. The difference of $t_{1/2}$ of nanocomposites with and without shear was significantly larger than that of neat iPP. The presence of GNSs and shear flow exhibited a synergistic interaction on promoting crystallization kinetics of iPP, although the effect of GNS concentration was not apparent. From WAXD results of isothermal and nonisothermal crystallization of sheared iPP, it was found that the appearance of β -crystals depended on the preservation of row nuclei, where the α -crystals were predominant in the iPP/GNSs nanocomposites, indicating that GNSs could directly induce α -crystals of iPP.



INTRODUCTION

It has been well documented that nanoparticles could act as effective nucleating agents for various semicrystalline polymers and affect the crystallization kinetics and crystalline morphology.^{1–10} For example, only 0.02 wt % multiwalled carbon nanotubes (CNTs) could reduce the half-crystallization time ($t_{1/2}$) of poly(L-lactide) to 9.6% when isothermally crystallized at 115 °C.¹¹ For nonisothermal crystallization at a cooling rate of 10 °C/min, the crystallization temperature of isotactic polypropylene (iPP) containing only 0.005 wt % gold nanoparticles was increased by 8.5 °C.¹² The similar nucleation effect was also found in other nanofillers, such as montmorillonite, zinc oxide, monodispersed SiO₂, etc.^{6,9,13} On the other hand, nanoparticles are prone to attract molecular chains and template the growth of polymer crystals. By appropriate lattice matching, a contact between polymer lamellae and substrate surface can be established, leading to the development of new crystalline morphology.^{5,7,8,14–17} One such morphology is the “nano-hybrid shish-kebabs” (NHSK) structure proposed by Li et al., where CNTs serve as the shish and disk-shaped polymer single crystals (kebabs) grow epitaxially perpendicular to the surface of CNTs.^{5,15}

In typical polymer processing operations (e.g., extrusion, injection, and blowing molding), the applications of different flow fields have great influence on the final crystallinity and crystalline morphology, which are intimately associated with their mechanical properties.^{18–22} Therefore, the subject of flow-induced crystallization and the relationship with the mechanical performances has attracted a great deal of attention in the community.^{23–29} It has been well established that shear flow can significantly enhance the crystallization kinetics of polymers. The accelerating effect can be attributed to the formation of oriented molecular chains, which nucleate and form crystal structure. The lifetime of the shear-induced precursors is closely related to the shear intensity and crystallization conditions. For example, the row nuclei can emerge under the effect of shear fields at low crystallization temperatures (T_c), while they would disintegrate into pointlike precursors at high T_c or relax after a long holding time.^{24–26} The shish structure can be formed by the

Received: December 9, 2010

Revised: March 10, 2011

Published: March 23, 2011

stable primary nuclei connected linearly along the flow direction and kebabs can be induced by shish afterward, which are oriented perpendicularly to the flow direction.²³ In the case of polymer processing, Bevis et al. reported that shear-controlled orientation injection molding led to more pronounced molecular orientation than conventional injection molding. The unique process made an 80% increase in Young's modulus and a 65% increase in tensile strength in resulting iPP compounds, which was attributed to the formation of the "shish-kebab" morphology.^{19,20}

For the development of new composite materials containing semicrystalline polymer matrix and nanoparticles, the combined effects of shear fields and nanoparticles on the crystallization behavior of polymers are of particular interest.³⁰ In this scenario, two kinds of nucleation origins can coexist: (1) homogeneous nucleating sites where shear-induced row nuclei or shish may occur; (2) heterogeneous nucleating sites which are facilitated by the presence of nanoparticles.³¹ The local velocity gradient may increase by orders of magnitude in the vicinity of nanoparticles, where the synergistic effect on the crystallization kinetics of polymer can be obtained. However, the presence of nanoparticles can also limit the motion of molecular chains, resulting in suppression of perfection and crystallinity of polymer crystals.^{7,32,33} Therefore, the existence of nanoparticles makes the shear-induced crystallization behavior much more complex than that in pure polymer system. For example, the nucleation efficiency of zinc oxide declined with the increase of shear rate because that there was the competition of nucleation density between zinc oxide nanoparticles and shear.⁹ However, in another study, the anisotropic nanoparticles, such as CNTs, were aligned along the shear direction, where the epitaxy growth of polymer crystals occurred. These oriented structures enhanced the properties of polymer matrix.^{7,31,33,34} This is also confirmed by the recent study of Fu et al., who reported the direct formation of NHSK in the injection-molded samples.³⁵ The lamellae of polyethylene showed a strong epitaxial growth on the surface of CNTs, where remarkable contribution of NHSK to the mechanical properties of PE was observed.

Graphene is a single atomic layer of carbon atoms tightly packed into the two-dimensional (2D) honeycomb structure. Because of its extraordinary electronic, thermal conductivity, and mechanical properties, graphene has been considered as an excellent candidate for nanoelectronic devices and nanoreinforcement in composite materials.^{36–41} Only a tiny fraction of graphene, generally less than 1 wt %, could cause a significant increase of mechanical and electrical properties of nanocomposites.^{36,39,42} For the further application of this unique nanomaterials in polymer composites, it is of great interest for us to understand the effect of graphene on polymer crystallization. In our previous study, we reported that 2D graphene nanosheets (GNSs) exhibited strong nucleating ability to accelerate the crystallization rate of poly-(L-lactide) under quiescent conditions, which could be attributed to surface-induced conformational order.¹⁰

This study aims at investigating the combined effects of 2D GNSs and shear flow on the crystallization behavior of isotactic polypropylene (iPP). In-situ synchrotron wide-angle X-ray diffraction (WAXD) and small-angle X-ray scattering (SAXS) techniques were employed to evaluate the crystallization kinetics and structure evolution in real time. In iPP, the most common modification, α -form, is a thermodynamically stable phase and has good mechanical strength; the β -form is a thermodynamically metastable phase and has better toughness than the α -form. The formation of β -form is strongly dependent on the process

conditions, such as flow fields and β -nucleating agents. The behavior of shear-induced crystallization and polymorphism in iPP has been extensively investigated, which enables us to better understand the combined effects of GNSs and shear fields on the crystallization behavior, such as crystallization kinetics and crystalline structure.

EXPERIMENTAL SECTION

Materials. The chosen iPP, model T30S, was provided by Dushanzi Petroleum Chemical Co., China, with a melt flow rate of 3 g/10 min (230 °C, 21.6 N), $M_w = 39.9 \times 10^4 \text{ g mol}^{-1}$, and $M_w/M_n = 4.6$. The mixed nanoparticles are graphene nanosheets (GNSs), which was feasibly dispersed in the solvent and improved interfacial interactions with polymer matrix in virtue of chemical functional groups.^{36,43–45} GNSs were synthesized from expanded graphite using the modified "Hummers" method in our laboratory; the details of the preparation scheme and the morphology of GNSs are introduced in the Supporting Information (SI).

Preparation of iPP/GNSs Nanocomposites. The solution blending method was utilized to prepare iPP nanocomposites with different GNSs contents. Taking the iPP/0.05 wt % GNSs nanocomposite sample as an example, the detailed sample preparation procedure was as follows: iPP (10 g) was dissolved in xylene (100 mL) at 130 °C by constant stirring in an oil bath. GNSs (5 mg) were dispersed in xylene (100 mL) and sonicated for 15 min to obtain a uniform dispersion. The mixture solution was subsequently obtained by adding the xylene/GNSs suspension into the xylene/iPP solution and continuously sonicated for another 15 min. Thereafter, the mixture was transferred to evaporating dishes, left overnight at room temperature, and dried in a vacuum oven at 80 °C for 2 days to evaporate the any residual solvent. Nanocomposite films (~0.5 mm thick) were prepared by molding the dried mixture at 200 °C for 10 min. iPP nanocomposites with 0.05 and 0.1 wt % GNSs were noted as PPG05 and PPG10, respectively, while neat iPP was noted as PPG0.

Synchrotron X-ray Characterization. WAXD and SAXS measurements were carried out at the Advanced Polymers Beamline (X27C, $\lambda = 0.1371 \text{ nm}$) in the National Synchrotron Light Source (NSLS), Brookhaven National Laboratory (BNL). A 2D MAR CCD X-ray detector (MAR-USA) with a resolution of 1024×1024 pixels (pixel size = $158.44 \mu\text{m}$) was used to acquire 2D-WAXD and 2D-SAXS images at 30 s intervals. An aluminum oxide (Al_2O_3) and a silver behenate (AgBe) standard were used to calibrate the detector distance for WAXD and SAXS, respectively.

2D-WAXD and 2D-SAXS patterns were integrated azimuthally with proper orientation correction to obtain their corresponding scattering profiles as a function of $|q| = 4\pi \sin \theta/\lambda$, where q is the first-order scattering vector, λ is the wavelength of X-ray beamline (0.1371 nm), and 2θ is the scattering angle. For integrated 1D-WAXD curves, a multi-peaks Gaussian fitting was used to obtain the areas of crystalline and amorphous peaks. The overall crystallinity (X_c) was calculated by

$$X_c = \frac{\sum A_{\text{cryst}}}{\sum A_{\text{cryst}} + \sum A_{\text{amorp}}} \quad (1)$$

where A_{cryst} and A_{amorp} represent the fitted areas of crystalline and amorphous phases, respectively. The normalized crystallinity (X_r) was used to estimate the crystallization kinetics of neat iPP and its GNSs nanocomposites by means of the following equation

$$X_r = \frac{X_c(t)}{X_c(\infty)} \quad (2)$$

where X_r is the normalized crystallinity of iPP and $X_c(t)$ and $X_c(\infty)$ are the fitting crystallinity of iPP at holding time (t) and the completion of

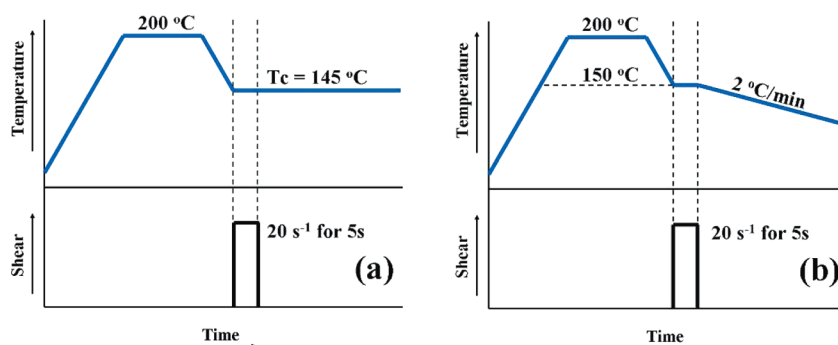


Figure 1. Schematic of shear conditions and thermal history as a function of time for WAXD and SAXS experiments: (a) isothermal crystallization and (b) nonisothermal crystallization.

Isothermal Crystallization under Quiescent Conditions

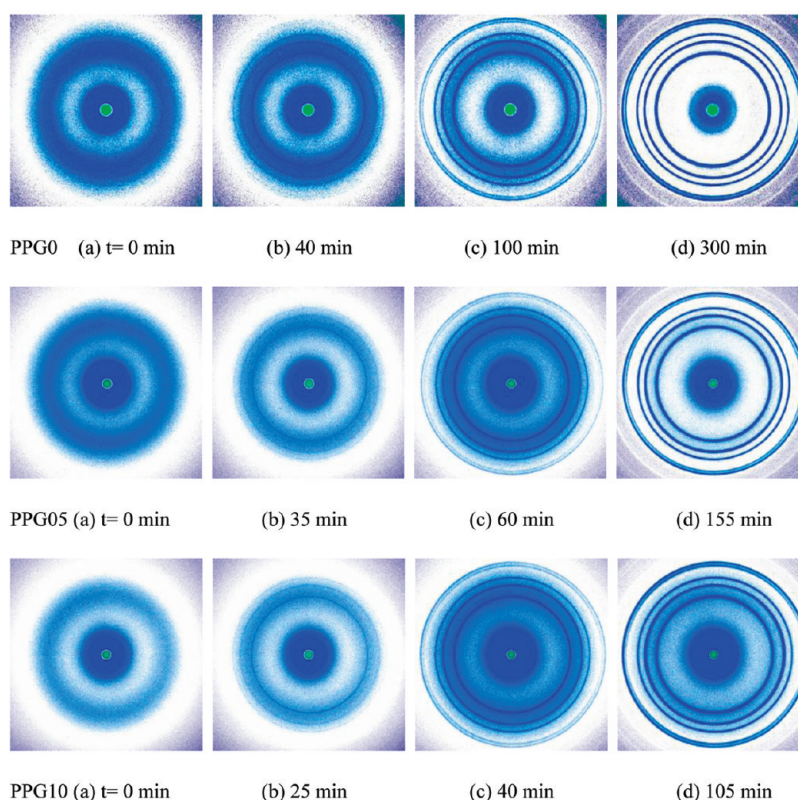


Figure 2. Selected 2D WAXD patterns of neat iPP and its GNSs nanocomposites isothermally crystallized at 145 °C under quiescent conditions.

crystallization, respectively. For 1D-SAXS data, the crystalline lamellar long period, $L_B = 2\pi/q$, was obtained.

Experimental Procedures. A Linkam CSS-450 high-temperature shearing stage, modified for in-situ X-ray scattering studies, was used to control the shear conditions and thermal history of polymer samples. For isothermal crystallization and nonisothermal crystallization, the experimental temperature profiles were set as shown in parts a and b of Figure 1, respectively, as described by the following profiles: (1) heating at 30 °C/min rate from room temperature to 200 °C; (2) holding the temperature at 200 °C for 300 s to eliminate any thermal history; (3) cooling at a rate of 30 °C/min down to 145 °C (150 °C); (4) imposing the shear at a rate of 20 s⁻¹ for 5 s and starting to gather 2D WAXD patterns at a interval of 30 s, when the temperature reaches 145 °C (150 °C); (5) holding the temperature at 145 °C until crystallization completed (isothermal

crystallization) or cooling at a rate of 2 °C/min to 80 °C (non-isothermal crystallization).

RESULTS

Isothermal Crystallization under Quiescent Conditions. In order to understand the role of GNSs in shear-induced crystallization of iPP nanocomposites, the nucleating ability of GNSs was first investigated under quiescent conditions. Figure 2 shows selected 2D WAXD patterns of neat iPP and its GNSs nanocomposites isothermally crystallized at 145 °C under quiescent conditions. A diffuse scattering ring is found in the first pattern ($t = 0$ min) of PPG0, indicating that no crystals are formed in the

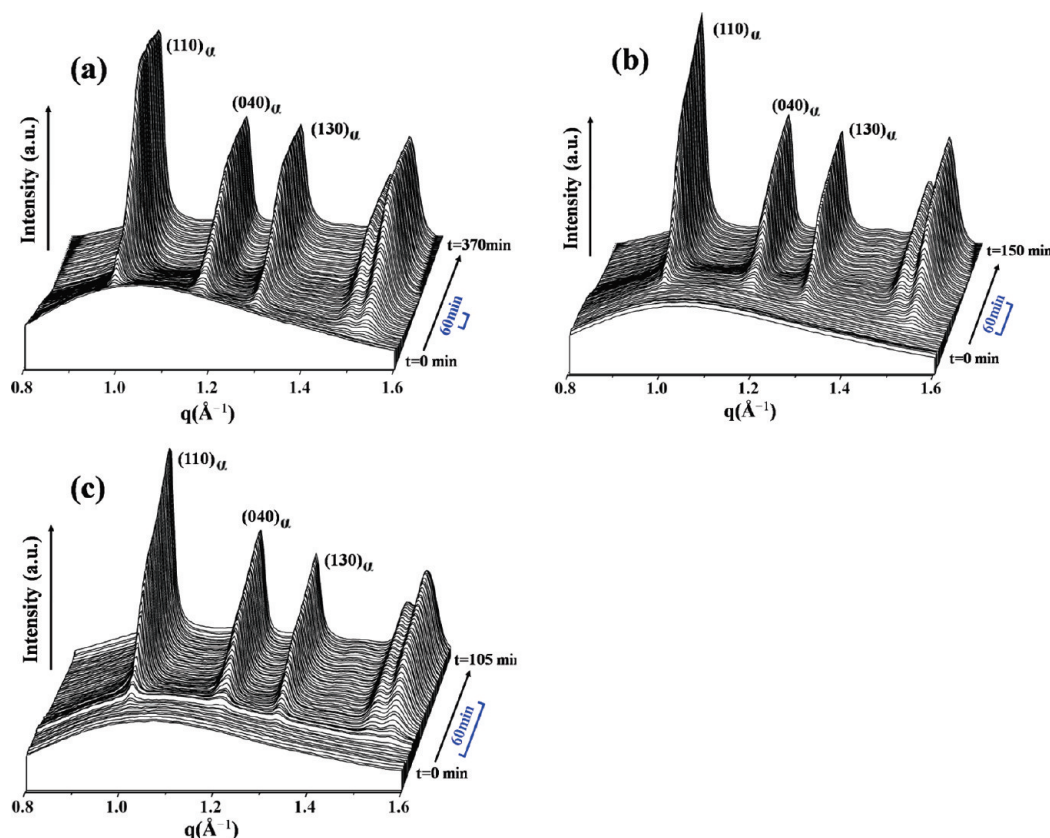


Figure 3. Time development of integrated 1D WAXD profiles of PPG0 (a), PPG05 (b), and PPG10 (c) isothermally crystallized at 145 °C under quiescent conditions.

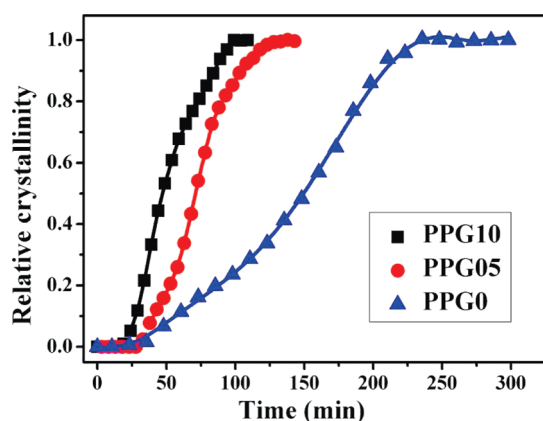


Figure 4. Normalized crystallinity of PPG0, PPG05, and PPG10 at 145 °C under quiescent conditions as a function of time.

iPP melt, which is also the case in PPG05 and PPG10. This confirms that the previous crystal structure of iPP was completely erased when cooled to the crystallization temperature (T_c). After an induction period, several isotropic crystal reflection pairs can be seen in all three samples, indicating the process of crystallization under quiescent conditions. The intensities of these isotropic diffraction peaks become stronger with time until the completion of crystallization. The time evolution of integrated 1D WAXD curves of PPG0, PPG05, and PPG10 is illustrated in Figure 3. It is seen that only α -crystal reflection peaks, corresponding to (110) , (040) , and (130) reflections, appear in all

three samples. By qualitatively comparing their time axis, the crystallization rates of iPP containing GNSs are evidently accelerated.

On the basis of eq 2, the normalized crystallinity of PPG0, PPG05, and PPG10 as a function of time is compiled in Figure 4 to evaluate the nucleating effect of GNSs on the crystallization kinetics of iPP. A typical sigmoidal evolution is seen in all three curves. From this figure, it can be concluded that the addition of GNSs significantly enhances the crystallization rate of iPP. Table 1 illustrates the crystallization half-time ($t_{1/2}$) of the three samples, where PPG05 and PPG10 are seen to reduce more than 50% of $t_{1/2}$ compared to that of PPG0, indicating the highly effective nucleation ability of GNSs. As shown in Figure S3, the high nucleation efficiency of GNSs is also confirmed through a nonisothermal crystallization process (at a cooling rate of 10 °C/min), where the crystallization temperatures of PPG05 and PPG10 are almost 10 °C higher than that of PPG0. As the GNSs content increases from 0.05 to 0.1 wt %, $t_{1/2}$ of the nanocomposites further decreases from 70.5 to 46.8 min. This proves that with the increasing nanofiller content more nucleation sites provided by GNSs can further shorten the induction period and accelerate the crystallization rate.

Isothermal Crystallization under Shear Flow. To investigate the combined effects of GNSs and shear on the crystallization of iPP, a step shear was applied to the supercooled iPP melt (see Figure 2a). Figure 5 illustrates selected 2D WAXD patterns of neat iPP and its GNSs nanocomposites isothermally crystallized at 145 °C after the cessation of shear. All three samples exhibit much shorter time to initiate crystalline reflections compared with those crystallized

under quiescent conditions. This observation also confirms that the application of shear plays an important role in promoting the crystallization of iPP. However, for PPG0, almost no anisotropic diffraction rings can be observed (Figure S4a). This can be understood for the following reasons. The applied shear is relatively weak (shear rate is 20 s^{-1} for 5 s duration), and the degree of supercooling is not too deep ($\Delta T = 20 \text{ }^{\circ}\text{C}$, as the normal melting temperature of α -iPP is $165 \text{ }^{\circ}\text{C}$). This results in high flexibility of polymer chains in a weakly oriented melt. The rapid relaxation of these chains leads to the formation of unoriented crystals. This is consistent with the stage of shear-induced oriented precursors break down into pointlike nuclei at high T_c , resulting in isotropic growth of iPP crystals.⁴⁶ In contrast, 2D WAXD patterns of PPG05 and PPG10 exhibit strong evidence of crystal orientation (see Figure 5b,c). Clear reflection arcs are seen in the meridian, indicating oriented crystals are formed. The orientation of these crystals is consistent with the epitaxial growth from the row nuclei; i.e., it is perpendicular to the flow direction. The growth of oriented crystals in

Table 1. Crystallization Half-Time ($t_{1/2}$) of PPG0, PPG05, and PPG10 Isothermally Crystallized at $145 \text{ }^{\circ}\text{C}$ under Quiescent Conditions and after Step Shear

	$t_{1/2}$ under quiescent conditions (min)	$t_{1/2}$ under shear conditions (min)
PPG0	150.3	29.5
PPG05	70.5	3.7
PPG10	46.8	2.6

PPG05 and PPG10 can be attributed to the combined effects of shear and GNSs. This phenomenon has also been observed in other system, where the stability of flow-induced precursors was found to improve in the presence of nanoparticles.³⁴ Because of the polymer chain and nanoparticle interaction, the precursor formation and the chain alignment can be enhanced, especially in the case of anisotropic nanoparticles. Under the shear field, the sheets of GNSs with the 2D flaky geometry are likely to align parallel along the flow direction and form an oriented network, where the motion of extended iPP chains is restricted. In other words, GNSs exhibit a synergistic effect with shear on promoting the crystallization and orientation of iPP crystals.

Figure 6 exhibits the time evolution of integrated 1D WAXD profiles of neat iPP and its GNSs nanocomposites isothermally crystallized at $145 \text{ }^{\circ}\text{C}$ after shear. For PPG0 (Figure 6a), only α -crystals appear, even though the shear flow often promotes the formation of β -crystals. As seen in Figure 5, the rapid relaxation of the row nuclei may occur in a low degree of supercooling; thus, the relaxed row nuclei would lose their β -nucleating ability.²⁷ It is interesting to note that a small fraction of β -crystals can be observed in PPG05 and PPG10 samples. We attribute this behavior to the restrictive effect of GNSs, which preserves the self-orientation nuclei (shish) that can induce the growth of β -crystals. This will be discussed later.

Figure 7 shows the normalized crystallinity as a function of time of PPG0, PPG05, and PPG10 after shear. As expected, clear enhancement of the crystallization kinetics of iPP is obtained in both neat iPP and its GNSs nanocomposites. As illustrated in Table 1, $t_{1/2}$ for PPG0 (29.5 min) after shear is reduced to about 20% of the value for

Isothermal Crystallization under Shear Flow

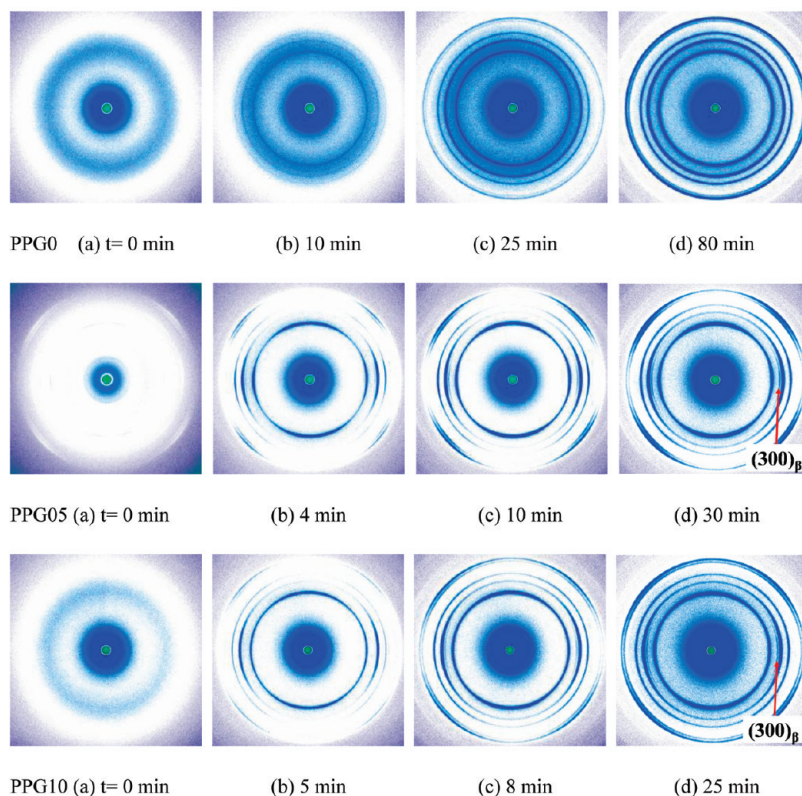


Figure 5. Selected 2D WAXD patterns of neat iPP and its GNSs nanocomposites isothermally crystallized at $145 \text{ }^{\circ}\text{C}$ after cessation of shear (at a shear rate of 20 s^{-1} for 5 s). The shear direction is vertical.

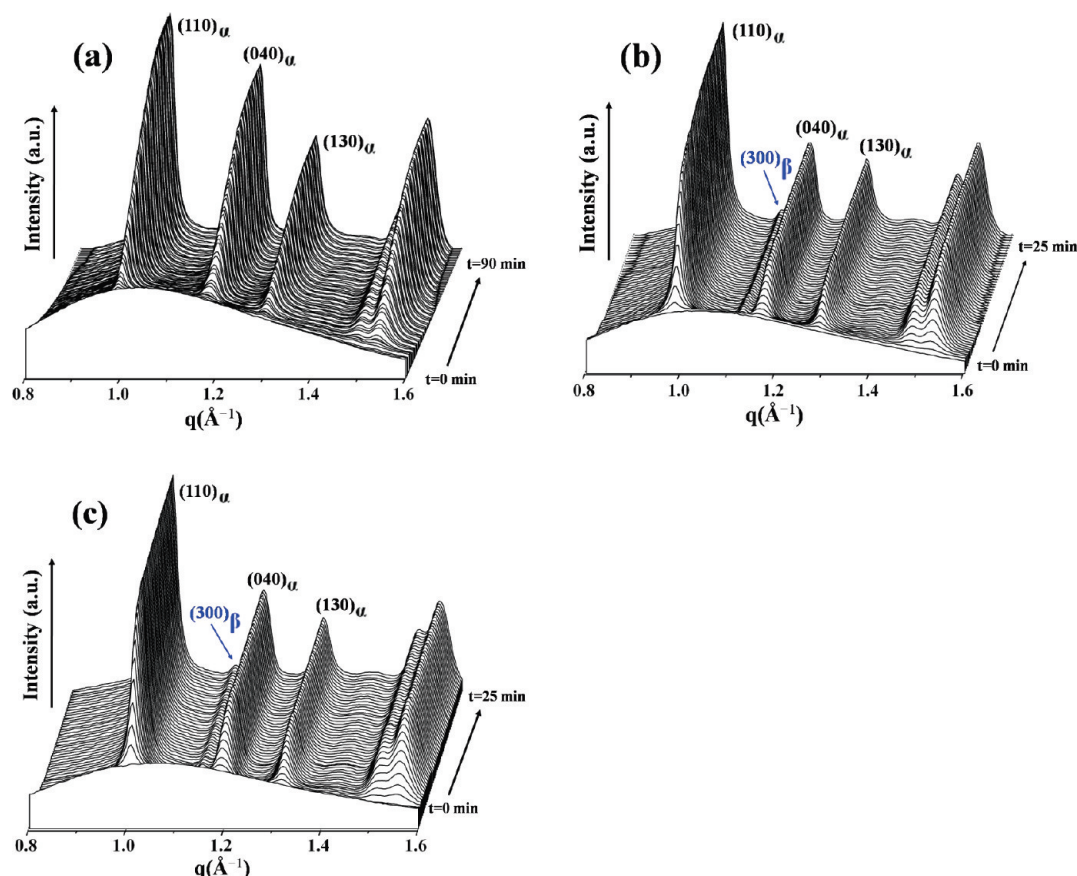


Figure 6. Time evolution of 1D WAXD profiles of PPG0 (a), PPG05 (b), and PPG10 (c) isothermally crystallized at 145 °C after the cessation of shear.

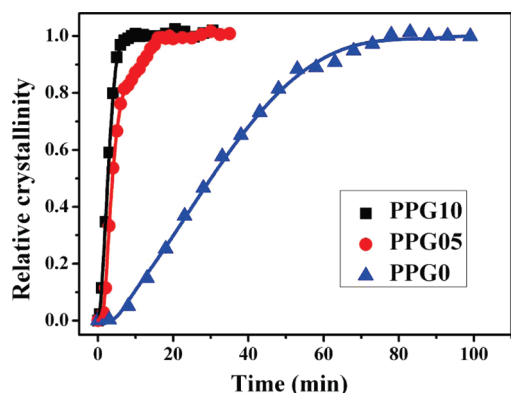


Figure 7. Normalized crystallinity of PPG0, PPG05, and PPG10 as a function of time, which were isothermally crystallized at 145 °C after the cessation of shear.

PPG0 under quiescent conditions. The crystallization rate of iPP/GNSs nanocomposites after shear, however, increases at least 18 times over that under quiescent conditions. This verifies that there is a synergistic effect of GNSs and shear on promoting the crystallization of iPP. Generally, the addition of nanoparticles can increase the viscosity of the system and prolong the relaxation time of molecular chains.^{33,47} Thus, it is logical to consider that the enhanced nucleating sites for growth of iPP crystals are not only composed of heterogeneous agents (GNSs) but also self-nucleation (rodlike nuclei or shish) induced by shear. These self-formation nuclei

(homogeneous nuclei) further accelerate the crystallization rate of PPG05 and PPG10 under shear field than those crystallized under quiescent conditions (Table 1). Under shear, the $t_{1/2}$ value of PPG05 and PPG10 changes from 3.7 to 2.6 min when the content of GNSs changes from 0.05 to 0.1 wt %. This indicates that the content effect of GNS on the crystallization rate under shear is not that pronounced.

To have a better comprehension of the structure development in iPP/GNSs nanocomposites during shear, in-situ SAXS measurement was carried out under the same thermomechanical conditions as in-situ WAXD measurement (Figure 2a). Figure 8 illustrates selected 2D SAXS patterns of neat iPP and its GNSs nanocomposites isothermally crystallized at 145 °C after shear. In all of the three systems, a pair of weak scattering maxima appears immediately in the meridian and becomes stronger with time. There is no sign of equatorial streak, which is probably because the size of the shish is too small and beyond the detection limit of SAXS.^{23,48,49} For PPG0, the 2D SAXS patterns indicate obvious structural anisotropy, rather different from corresponding 2D WAXD results (Figure 5). The reason for these differences may be partially due the different detecting scales of WAXD and SAXS measurements.^{23,49,50} However, it is also conceivable that although the crystal structure appears to be randomly arranged, the large arrangement of lamellae possess some preferred orientation. The vertical (meridional) scattering streak indicates that the shear-induced oriented structures are preserved at high T_c even after subsequent crystallization.

Time-resolved integrated 1D SAXS profiles of neat iPP and its nanocomposites isothermally crystallized at 145 °C after shear

are illustrated in Figure 9. It is shown that the scattered intensity gradually increases with time for all three systems, and it reaches a plateau value, indicating the completion of crystallization. All profiles in Figures 9a–c are plotted in the same time scale, where we can conclude that GNSs show strong ability to enhance the

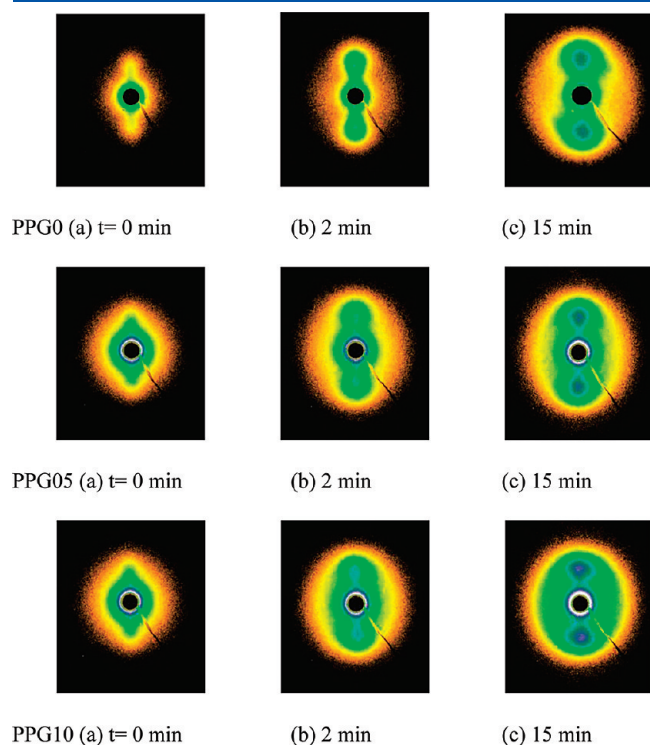


Figure 8. Selected 2D SAXS patterns of neat iPP and iPP/GNSs nanocomposites isothermally crystallized at 145 °C after the cessation of shear (at a rate of 20 s^{−1} for 5 s).

crystallization rate of iPP, which is consistent with the WAXD results.

Figure 10 illustrates the changes of average spacing between the adjacent lamellae (i.e., long period, L_B) in PPG0, PPG05, and PPG10. In all three systems, L_B is found to decrease rapidly at the early stage of crystallization and then reaches a plateau value at the late stage (e.g., L_B of PPG05 decreases from 36.9 to 22.4 nm). It is further noted that L_B for PPG05 (22.4 nm) and PPG10 (23.0 nm) is slightly smaller than that for PPG0 (24.6 nm). This observation indicates that higher nucleation density (due to the presence of GNSs) leads to smaller long period.⁴⁸ The difference between the plateau values of L_B for PPG0, PPG05, and PPG10 confirms that GNSs are good nucleating agent for iPP crystallization even under shear.

DISCUSSION

The results described above provided a microscopic insight into the crystallization behavior of iPP/GNSs nanocomposites under shear. First, the $t_{1/2}$ values of PPG05 and PPG10 crystallized under quiescent conditions were found to decrease by at least 50% compared with that of PPG0 ($t_{1/2} = 150.3$ min), indicating that GNSs are effective nucleating agents for iPP crystallization. As revealed by atomic force microscopic image in Figure S1, the average length (0.87 μm) of GNSs is nearly 3 orders of magnitude greater than the average thickness (1–2 nm), confirming that GNSs are 2D nanosheets with a very large specific surface area. With such geometry, the molecular chains are prone to interact with the surface of GNSs and reduce the nucleation barrier of iPP. In our previous study, we concluded that GNSs played an important role in prepacking conformational ordering frame of poly(L-lactide) chains prior to the advent of crystallization.¹⁰ From the changing sequence of conformational and crystalline characteristic bands, we further concluded that GNSs acted as a template for PLLA chains to land on, leading to the phenomenon of surface-induced conformational

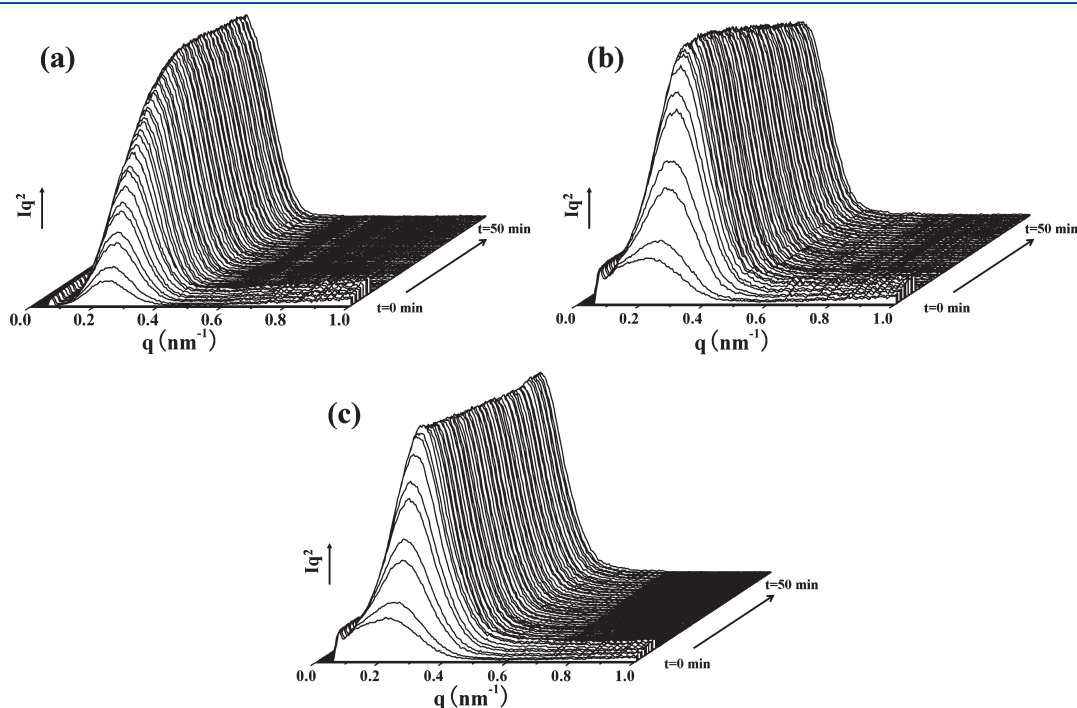


Figure 9. Time-resolved integrated 1D SAXS profiles of PPG0 (a), PPG5 (b), and PPG10 (c) isothermally crystallizing at 145 °C after shear.

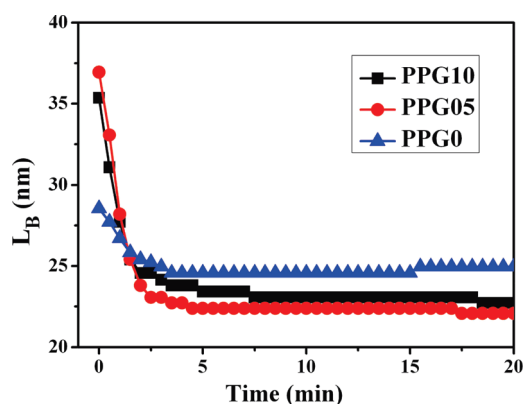


Figure 10. Plots of long period as a function of crystallization time for PPG0, PPG05, and PPG10 after the cessation of shear.

order (SICO). Recently, Lu et al. reported that the protruding methyl groups of iPP could also interact with the graphite layer of CNTs, resulting in the adsorption of iPP chains on the surface of CNTs.⁵¹ Structurally, CNTs and GNSs are composed of the same molecular unit (i.e., graphite layers of sp^2 -bonded carbon). Hence, it is reasonable to argue that there are also interactions between GNSs and iPP chains. It is conceivable that the surface of GNSs can attract nearby iPP chains, allowing them to form a conformational ordered structure that would trigger the crystallization process. As a result, both induction period and crystallization rate of iPP can be significantly affected. With the increase of GNSs loading, more nucleation sites can be provided thus greatly enhancing the crystallization rate of iPP.

When a relatively weak shear field (at a rate of 20 s^{-1} for 5 s) is applied, the crystallization kinetics of all three systems is accelerated (see Table 1). For PPG0 crystallized after the cessation of shear, isotropic diffraction rings (instead of anisotropic scattering features) are seen (Figure 5). This may be explained as follows. Generally, only polymer molecules above the “critical orientation molecular weight” (M^*) could remain oriented after shear at a given shear rate ($\dot{\gamma}$), following the relationship $M^* \propto (\dot{\gamma})^{-\alpha}$ where α is a positive exponent.⁵² The memory of the flow field can be erased if the sheared sample is kept quiescently at a high temperature for a sufficient long time. This is because the flow-induced precursors are intrinsically unstable at high temperatures.²⁵ Considering the case of sheared PPG0, the sample was crystallized at a low degree of supercooling ($\Delta T = 20\text{ }^\circ\text{C}$), where the mobility of iPP chains was high. This would result in an isotropic crystal structure due to two possibilities: (1) the relaxation of shear-induced row nuclei leads to a random crystal structure (this has also been found in the studies of poly(butylene terephthalate) and isotactic polystyrene.^{24,53}); (2) the size and concentration of oriented crystals are too small to be detected by WAXD. However, the lamellar structure could remain with certain degree of orientation in the flow direction, which is observable by SAXS (Figure 8).

For PPG05 and PPG10 crystallized after shear, it was found that anisotropic diffraction rings appeared clearly in 2D WAXD patterns (Figure 5). The arclike diffractions (e.g., the $(110)_\alpha$ reflection) in the meridian indicated that the oriented crystals were formed parallel to the flow direction. This observation confirms that GNSs dramatically enhance the crystallization kinetics and also affect the morphology. Recently, García-Gutiérrez et al. also reported that the orientation of poly(butylene terephthalate) crystals under shear changed dramatically in the

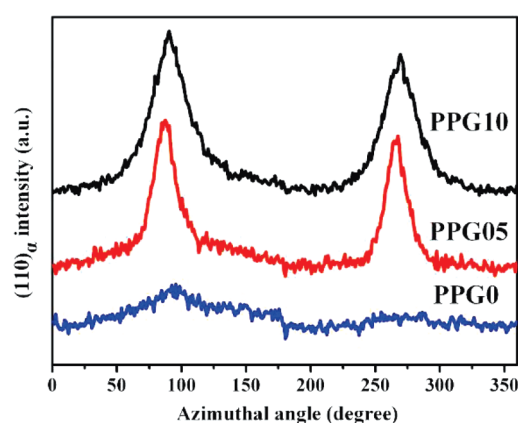


Figure 11. Azimuthal profiles of 2D WAXD patterns at the $(110)_\alpha$ reflection for PPG0, PPG05, and PPG10 in the initial stage of crystallization.

presence of CNTs.⁷ Both poly(butylene terephthalate) chains and CNTs were found to align along the flow direction. The epitaxial crystallization of PBT was able to occur on the surface of CNTs, resulting in the NHSK structure. Compared with CNTs, GNSs exhibit 2D flaky geometry. The direct formation of NHSK structure seems to be unreasonable because the length of GNSs (about $0.87\text{ }\mu\text{m}$) is too large for kebabs to vegetate, but the epitaxial growth of iPP on the surface of GNSs is evident due to the significant increase of crystallization rate of iPP under quiescent conditions. In addition, it is well-known that a network structure can be formed by the interactions of nanoparticles in the polymer matrix, where this network also restricts the motion of molecular chains.^{4,9,31,33,34,47,54} With the application of shear, the isotropic network structure (due to the nanoparticle interactions) can transform into an anisotropic one, where some GNSs sheets become parallel to the flow direction, allowing some iPP chains to also align accordingly. Additionally, the relaxation time of the oriented polymer chains is prolonged due to the restriction effect of GNSs, where the row nuclei can survive longer and evolve into the shish entity.

There should be two kinds of nucleating sites in sheared PPG05 and PPG10. One is the heterogeneous nucleating sites provided by GNSs, which are inclined to align along the flow field. The other is the self-nucleating sites (or homogeneous nucleating sites, in the form of row nuclei) due to the effect of shear. By the cooperative interactions of these two nucleating sites, faster crystallization kinetics can be induced in sheared PPG05 and PPG10 when compared to that in sheared PPG0. The WAXD results strongly suggest that there is a synergistic effect of GNSs and shear flow on the crystallization behavior of iPP. Meanwhile, the relatively small dependence of crystallization rate of iPP on the concentration of GNSs may be due to the limited amount of preserved row nuclei formed in the GNSs network (Figure 7 and Table 1).

From Figure 6, another phenomenon was noted that was the appearance of β -crystals in both iPP/GNSs nanocomposite samples (however, no β -crystals was formed in pure iPP). Naturally, one might ask what role did GNSs play in the formation of β -crystals under shear? In order to answer this question, we first discuss why there was no β -crystals found in the sheared PPG0. Figure 11 illustrates the azimuthal profiles of 2D WAXD patterns of PPG0 for the $(110)_\alpha$ reflection at the initial stage of isothermal crystallization after shear. As stated

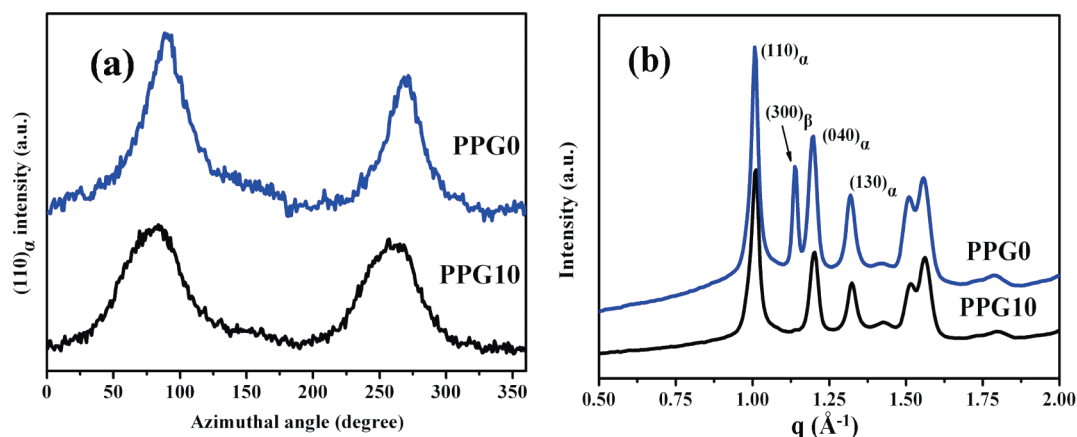


Figure 12. Initial azimuthal distribution for $(110)_\alpha$ reflection (a) and final integrated 1D WAXD profiles of PPG0 and PPG10 (b) during nonisothermal crystallization process after the cessation of shear (20 s^{-1} for 5 s at 150°C).

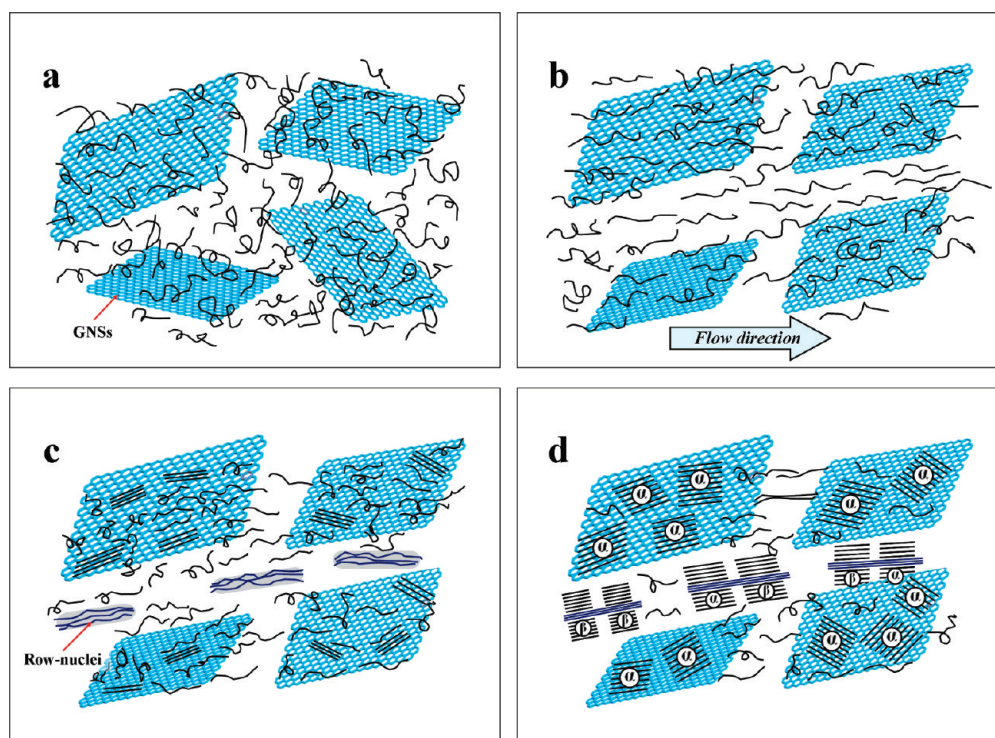


Figure 13. Schematic diagrams of crystallization process of iPP under the combined action of GNSs and shear flow.

earlier, row nuclei can relax into pointlike nuclei in sheared PPG0 at high temperature, causing the isotropic crystal growth (Figure 5), whereas large orient lamellar structures are also present in large scales (Figure 8). A similar phenomenon has been reported before. Varga et al. reported that by pulling the glass fiber in iPP melt α row-nuclei could be developed, which surface could induce the growth of β -crystals leading to the formation of cylindrite.²⁷ However, the capability of α row nuclei to induce β -crystals was lost by repeatedly crystallizing and melting. In this study, the relaxation of row nuclei may also decrease the ability to induce β -crystals. Therefore, only the α -crystals appeared in PPG0 isothermally crystallized after shear. While in PPG05 and PPG10, relatively strong anisotropy could be observed at the initial stage of crystallization, which also

suggests that oriented nuclei play an important role in the formation of β -crystals.

To further investigate the origin of β -crystals, a nonisothermal crystallization experiment was carried out as depicted in Figure 2b. The nonisothermal condition was expected to preserve row nuclei by subsequent cooling after shear. Figure 12a shows the initial azimuthal distribution of PPG0 ($t = 4 \text{ min}$) and PPG10 ($t = 3 \text{ min}$) in this study, where clear crystal orientation is observed in PPG0, verifying that shear induced row nuclei were retained and further developed into oriented crystals. The final integrated 1D WAXD profiles of PPG0 and PPG10 at the end the nonisothermal study (80°C) are shown in Figure 12b. It is seen that a fair amount of β -crystals emerges in PPG0. This evidence definitively confirms that row nuclei survived by the cooling treatment,

where the presence of row nuclei induced β -crystals. However, although anisotropy in crystal structure is observed at the initial period of crystallization in PPG10, no detectable β -crystals can be observed. This means that the influence of GNSs on the formation of α -crystals overwhelms that of β -crystals, which can be induced by the survival of row nuclei. It is conceivable that the heterogeneous GNS nucleating sites are not in favor of the formation of β -crystals.

According to the results above, the following conclusions can be drawn as follows. GNSs have a strong ability to induce the crystallization of α -crystals, while the application of shear can induce row nuclei. However, the stability of the row nuclei is enhanced by the confinement of the GNSs network, thus holding the ability to induce β -crystals. There is a direct competition between the two nucleating sites (GNSs and row nuclei of iPP). GNSs manifest more potential on the nucleation ability for iPP than row nuclei induced by shear. As a result, when shear is applied to iPP/GNSs nanocomposites, the dominant formation of α -crystals can be attributed to the nucleation by GNSs. The appearance of a small amount of β -crystals is due to the row nuclei survived through the restricting effect of GNSs network on molecular chains.

The crystallization process of sheared iPP melt in the presence of GNSs is schematically illustrated in Figure 13. Before the application of shear, nanosheets of GNSs construct an isotropic network in the matrix of random iPP chains (Figure 13a). During shear, both GNSs and iPP chains tend to align along the flow direction. The isotropic GNSs network thus transforms into an anisotropic one as shown in Figure 13b. Subsequently, due to the restriction of GNSs layers, the relaxation of the molecular chains between the adjacent nanosheets is hindered and the oriented chains evolve into row-nuclei, which may grow into shish (Figure 13c). Both GNSs and row nuclei (or shish) having different nucleation ability would induce crystallization of surrounding iPP chains at the same time. Eventually, GNSs and shear exhibit a synergistic effect on accelerating crystallization kinetics of iPP. Because of the stronger nucleation ability of GNSs, the majority of the crystallinity is due to α -crystals, and only a small amount of β -crystals is formed due to the presence of row nuclei (or shish) (Figure 13d).

CONCLUSIONS

The combined effect of GNSs and shear flow on the crystallization behavior of iPP was investigated, where 2D GNSs was prepared by the modified Hummer's method. The nucleating ability of GNSs was first determined under quiescent conditions. The addition of GNSs efficiently accelerated the crystallization rate of iPP, where the crystallization half-time ($t_{1/2}$) of the nanocomposites containing 0.05 and 0.1 wt % GNSs was reduced at least 50% compared to that of neat iPP. As the content of GNSs was increased from 0.05 to 0.1 wt %, the $t_{1/2}$ value was further shortened. A relatively weak shear (at a rate of 20 s^{-1} for 5 s) was imposed to the iPP melt at a low degree of supercooling ($T_c = 145^\circ\text{C}$). An isotropic growth of α -crystals appeared in neat iPP, which could be attributed to the relaxation of low oriented row nuclei, whereas for iPP/GNSs nanocomposites, the WAXD results showed strong evidence of crystal orientation. After shear, the isotropic network of GNSs transformed into an anisotropic one, where the mobility of iPP chains was restricted by the adjacent nanosheets. Therefore, the lifetime of row nuclei was prolonged. GNSs presented an amplification effect of shear on

the shear-induced row nuclei and orientation of iPP crystals. Two kinds of nucleating origins coexisted in sheared nanocomposites. One was heterogeneous nucleating sites (2D GNSs) aligning along the flow field. The other was self-nucleating sites (row-nuclei) induced by shear and survived in the GNSs network. As a result, the difference of $t_{1/2}$ of nanocomposites with and without shear was larger than that of neat iPP. GNSs and shear flow exhibited a synergistic effect on promoting the crystallization kinetics of iPP (however, the kinetics is not strongly GNS concentration dependent). From the WAXD results of isothermal and nonisothermal crystallization of sheared iPP, it was confirmed that the appearance of β -crystals depended on the preservation of row nuclei. However, α -crystals were predominant in iPP/GNSs nanocomposites, even though some row nuclei were expected to survive. It was suggested that the effect of GNSs to induce α -crystals of iPP is the dominant factor. The results from this study offered helpful guidance to control the crystalline structure of iPP/GNSs nanocomposites.

ASSOCIATED CONTENT

S Supporting Information. Detailed preparation process of graphene nanosheets; AFM image of GNSs; XPS spectra of GNSs; complex viscosity and storage modulus of PPG10 and PPG0; DSC curves and corresponding azimuthal distribution for $(110)_\alpha$ reflection of PPG0, PPG05, and PPG10. This material is available free of charge via the Internet at <http://pubs.acs.org>.

AUTHOR INFORMATION

Corresponding Author

*E-mail: zmli@scu.edu.cn (Z.-M.L.), bhsiao@notes.cc.sunysb.edu (B.S.H.).

ACKNOWLEDGMENT

The authors are indebted to Dr. Lixia Rong and Jie Zhu from Synchrotron Light Source, Brookhaven National Laboratory (USA), for their help of WAXS measurement. The Chinese team thanks the financial support by the National Outstanding Youth Foundation of China (Grant No. 50925311) and the State Key Program of National Natural Science of China (Grant No. 51033004), and the US team thanks the financial support by the National Science Foundation of the US (DMR-0906512).

REFERENCES

- (1) Grady, B. P.; Pompeo, F.; Shambaugh, R. L.; Resasco, D. E. *J. Phys. Chem. B* **2002**, *106*, 5852–5858.
- (2) Ray, S. S.; Okamoto, M. *Prog. Polym. Sci.* **2003**, *28*, 1539–1641.
- (3) Sandler, J. K. W.; Pegel, S.; Cadek, M.; Gojny, F.; van Es, M.; Lohmar, J.; Blau, W. J.; Schulte, K.; Windle, A. H.; Shaffer, M. S. P. *Polymer* **2004**, *45*, 2001–2015.
- (4) Xu, J. T.; Zhao, Y. Q.; Wang, Q.; Fan, Z. Q. *Macromol. Rapid Commun.* **2005**, *26*, 620–625.
- (5) Li, L. Y.; Li, C. Y.; Ni, C. Y. *J. Am. Chem. Soc.* **2006**, *128*, 1692–1699.
- (6) Ke, Y. C.; Wu, T. B.; Xia, Y. F. *Polymer* **2007**, *48*, 3324–3336.
- (7) Garcia-Gutierrez, M. C.; Hernandez, J. J.; Nogales, A.; Pantine, P.; Rueda, D. R.; Ezquerro, T. A. *Macromolecules* **2008**, *41*, 844–851.
- (8) Hu, X.; An, H. N.; Li, Z. M.; Geng, Y.; Li, L. B.; Yang, C. L. *Macromolecules* **2009**, *42*, 3215–3218.
- (9) D'Haese, M.; Van Puyvelde, P.; Langouche, F. *Macromolecules* **2010**, *43*, 2933–2941.

- (10) Xu, J. Z.; Chen, T.; Yang, C. L.; Li, Z. M.; Mao, Y. M.; Zeng, B. Q.; Hsiao, B. S. *Macromolecules* **2010**, *43*, 5000–5008.
- (11) Xu, H. S.; Dai, X. J.; Lamb, P. R.; Li, Z. M. *J. Polym. Sci., Part B: Polym. Phys.* **2009**, *47*, 2341–2352.
- (12) Masirek, R.; Szkudlarek, E.; Piorkowska, E.; Slouf, M.; Kratochvil, J.; Baldrian, J. *J. Polym. Sci., Part B: Polym. Phys.* **2010**, *48*, 469–478.
- (13) Krikorian, V.; Pochan, D. J. *Macromolecules* **2005**, *38*, 6520–6527.
- (14) Haubruge, H. G.; Daussin, R.; Jonas, A. M.; Legras, R.; Wittmann, J. C.; Lotz, B. *Macromolecules* **2003**, *36*, 4452–4456.
- (15) Li, C. Y.; Li, L. Y.; Cai, W. W.; Kodjie, S. L.; Tenneti, K. K. *Adv. Mater.* **2005**, *17*, 1198–1202.
- (16) Haggemueller, R.; Fischer, J. E.; Winey, K. I. *Macromolecules* **2006**, *39*, 2964–2971.
- (17) Strawhecker, K. E.; Manias, E. *Chem. Mater.* **2003**, *15*, 844–849.
- (18) Kmetty, Á.; Bárány, T.; Karger-Kocsis, J. *Prog. Polym. Sci.* **2010**, *35*, 1288–1310.
- (19) Kalay, G.; Bevis, M. J. *J. Polym. Sci., Part B: Polym. Phys.* **1997**, *35*, 241–263.
- (20) Kalay, G.; Bevis, M. J. *J. Polym. Sci., Part B: Polym. Phys.* **1997**, *35*, 265–291.
- (21) Zhong, G. J.; Li, L. B.; Mendes, E.; Byelov, D.; Fu, Q.; Li, Z. M. *Macromolecules* **2006**, *39*, 6771–6775.
- (22) Wang, Y.; Pan, J. L.; Mao, Y. M.; Li, Z. M.; Li, L. B.; Hsiao, B. S. *J. Phys. Chem. B* **2010**, *114*, 6806–6816.
- (23) Somani, R. H.; Yang, L.; Hsiao, B. S.; Agarwal, P. K.; Fruitwala, H. A.; Tsou, A. H. *Macromolecules* **2002**, *35*, 9096–9104.
- (24) Li, L. B.; de Jeu, W. H. *Macromolecules* **2004**, *37*, 5646–5652.
- (25) Azzurri, F.; Alfonso, G. C. *Macromolecules* **2005**, *38*, 1723–1728.
- (26) Kumaraswamy, G.; Issaian, A. M.; Kornfield, J. A. *Macromolecules* **1999**, *32*, 7537–7547.
- (27) Varga, J.; KargerKocsis, J. *J. Polym. Sci., Part B: Polym. Phys.* **1996**, *34*, 657–670.
- (28) Hashimoto, T.; Murase, H.; Ohta, Y. *Macromolecules* **2010**, *43*, 6542–6548.
- (29) Kolnaar, J. W. H.; Keller, A. *Polymer* **1994**, *35*, 3863–3874.
- (30) Jancar, J.; Douglas, J. F.; Starr, F. W.; Kumar, S. K.; Cassagnau, P.; Lesser, A. J.; Sternstein, S. S.; Buehler, M. J. *Polymer* **2010**, *51*, 3321–3343.
- (31) Rozanski, A.; Monasse, B.; Szkudlarek, E.; Pawlak, A.; Piorkowska, E.; Galeski, A.; Haudin, J. M. *Eur. Polym. J.* **2009**, *45*, 88–101.
- (32) Hwang, W. R.; Peters, G. W. M.; Hulsen, M. A.; Meijer, H. E. H. *Macromolecules* **2006**, *39*, 8389–8398.
- (33) Patil, N.; Balzano, L.; Portale, G.; Rastogi, S. *Carbon* **2010**, *48*, 4116–4128.
- (34) Patil, N.; Balzano, L.; Portale, G.; Rastogi, S. *Macromolecules* **2010**, *43*, 6749–6759.
- (35) Yang, J. H.; Wang, C. Y.; Wang, K.; Zhang, Q.; Chen, F.; Du, R. N.; Fu, Q. *Macromolecules* **2009**, *42*, 7016–7023.
- (36) Stankovich, S.; Dikin, D. A.; Dommett, G. H. B.; Kohlhaas, K. M.; Zimney, E. J.; Stach, E. A.; Piner, R. D.; Nguyen, S. T.; Ruoff, R. S. *Nature* **2006**, *442*, 282–286.
- (37) Geim, A. K.; Novoselov, K. S. *Nature Mater.* **2007**, *6*, 183–191.
- (38) Gilje, S.; Han, S.; Wang, M.; Wang, K. L.; Kaner, R. B. *Nano Lett.* **2007**, *7*, 3394–3398.
- (39) Rao, C. N. R.; Sood, A. K.; Subrahmanyam, K. S.; Govindaraj, A. *Angew. Chem., Int. Ed.* **2009**, *48*, 7752–7777.
- (40) Novoselov, K. S.; Geim, A. K.; Morozov, S. V.; Jiang, D.; Zhang, Y.; Dubonos, S. V.; Grigorieva, I. V.; Firsov, A. A. *Science* **2004**, *306*, 666–669.
- (41) Li, D.; Kaner, R. B. *Science* **2008**, *320*, 1170–1171.
- (42) Liang, J. J.; Huang, Y.; Zhang, L.; Wang, Y.; Ma, Y. F.; Guo, T. Y.; Chen, Y. S. *Adv. Funct. Mater.* **2009**, *19*, 2297–2302.
- (43) Paredes, J. I.; Villar-Rodil, S.; Martinez-Alonso, A.; Tascon, J. M. D. *Langmuir* **2008**, *24*, 10560–10564.
- (44) Stankovich, S.; Piner, R. D.; Chen, X. Q.; Wu, N. Q.; Nguyen, S. T.; Ruoff, R. S. *J. Mater. Chem.* **2006**, *16*, 155–158.
- (45) Ramanathan, T.; Abdala, A. A.; Stankovich, S.; Dikin, D. A.; Herrera-Alonso, M.; Piner, R. D.; Adamson, D. H.; Schniepp, H. C.; Chen, X.; Ruoff, R. S.; Nguyen, S. T.; Aksay, I. A.; Prud'homme, R. K.; Brinson, L. C. *Nature Nanotechnol.* **2008**, *3*, 327–331.
- (46) Nogales, A.; Mitchell, G. R. R.; Vaughan, A. S. *Macromolecules* **2003**, *36*, 4898–4906.
- (47) Wang, K.; Xiao, Y.; Na, B.; Tan, H.; Zhang, Q.; Fu, Q. *Polymer* **2005**, *46*, 9022–9032.
- (48) Yang, L.; Somani, R. H.; Sics, I.; Hsiao, B. S.; Kolb, R.; Fruitwala, H.; Ong, C. *Macromolecules* **2004**, *37*, 4845–4859.
- (49) Somani, R. H.; Yang, L.; Hsiao, B. S.; Sun, T.; Pogodina, N. V.; Lustiger, A. *Macromolecules* **2005**, *38*, 1244–1255.
- (50) Wang, Z. G.; Hsiao, B. S.; Sirota, E. B.; Agarwal, P.; Srinivas, S. *Macromolecules* **2000**, *33*, 978–989.
- (51) Lu, K. B.; Grossiord, N.; Koning, C. E.; Miltner, H. E.; van Mele, B.; Loos, J. *Macromolecules* **2008**, *41*, 8081–8085.
- (52) Somani, R. H.; Hsiao, B. S.; Nogales, A.; Srinivas, S.; Tsou, A. H.; Sics, I.; Balta-Calleja, F. J.; Ezquerro, T. A. *Macromolecules* **2000**, *33*, 9385–9394.
- (53) Gutierrez, M. C. G.; Alfonso, G. C.; Riekel, C.; Azzurri, F. *Macromolecules* **2004**, *37*, 478–485.
- (54) Dykes, L. M. C.; Torkelson, J. M.; Burghardt, W. R.; Krishnamoorti, R. *Polymer* **2010**, *51*, 4916–4927.